GSA Data Repository Item DR2006161

Topographic advection on fault-bend folds: Inheritance of valley positions and the formation of wind gaps

S.R. Miller and R.L. Slingerland
Department of Geosciences, Pennsylvania State University, University Park, Pennsylvania 16802, USA; email: srmiller@geosc.psu.edu

APPENDIX DR1. Topographic cross-correlation

Swath topographic profiles of mean elevation measured the length of ridge flanks—either the proximal or distal side as defined in the paper—demarcate the general positions of transversely oriented valleys and interfluves along linear ridge segments. For this, we used 3 arc-second SRTM digital elevation models projected into the local UTM projection and resampled at a 90 m resolution. Swath profiles were produced by averaging elevation data sampled parallel to the direction of hanging-wall motion, extending from crest to base of each ridge. Averaging was done parallel to this direction, rather than perpendicular to the ridge trend or thrust fault strike, because slip on these faults is locally oblique (Mugnier et al., 1999). Study areas and the exact regions from which profiles were extracted are shown in Figure DR1. Averaging in the direction of hanging-wall motion yielded approximately strike-wise topographic swath profiles where lows and highs represent transverse valleys and ridges, respectively (Fig. DR2). Wind gaps and peaks are evident in the ridge-line profile and commonly correspond spatially with valleys and ridges on the proximal and distal ridge flanks. For better comparison against model results (e.g., the null hypothesis simulation cross-correlation results in Fig. DR3), profiles were smoothed with a 500 m-wide moving averaging window.

Topographic profiles from the two opposing ridge flanks were then cross-correlated without a lag across the principal drainage divide, yielding a Pearson product-moment correlation coefficient, r (Davis, 1973; Borradaile, 2003).

Range width and drainage divide position depend on parameters N_e and α. Because simulated steady-state topography is sensitive to initial conditions and strict comparisons of correlation coefficient among individual simulations with different input

parameters is not meaningful, we used a Monte Carlo approach to constrain model uncertainty and therefore better assess comparisons among model results (Borradaile, 2003). For each set of parameters, multiple realizations of each model (n = 10–200 depending on computational cost) were created using different horizontal initial surfaces of randomly perturbed node elevations. In our study, we intended not to determine if a given correlation coefficient was significant such as by using a t-test (Davis, 1973), but rather to determine if the correlation coefficient associated with certain model parameters was significantly different from the null hypothesis (i.e., r for simulations with no horizontal bedrock motion).

APPENDIX DR2. Model description

Bedrock streamlines are controlled in the landscape evolution model by simple kinematic rules following Suppe (1983). Rock streamlines parallel the fault everywhere and bedrock has a velocity of V. This rate is equivalent to the fault-slip rate. Velocities change direction, but not magnitude, across axial surfaces. The dips of the detachments or flats are 0°; α is ramp dip and β is the axial surface dip, where $\beta = (180-\alpha))/2$. Above the fault ramp, the horizontal component, v, is defined as

$$v = V \cos\alpha \tag{A1}$$

The vertical component, u, is defined as

$$u = V \sin\alpha \tag{A2}$$

Note that this notation goes against the convention in physics where u is the x-directed velocity but conforms with common geologic usage where u is uplift rate.

The rate of fluvial erosion in bedrock channels is assumed to be proportional to unit stream power (Howard et al., 1994). Erosion rate, E, has units of $m \cdot yr^{-1}$ and is defined as

$$E = k_b \frac{Q}{W} S \tag{A3}$$

where k_b is the intrinsic erodibility (m^{-1}), Q is total water discharge ($m^3 \cdot yr^{-1}$), W is stream width (m), and S is stream slope (unitless).

We rewrite the stream power law in terms of upstream drainage area in order to allow simpler comparison with sites where area is readily measurable from DEMs but Q is not. Hydrologic and hydraulic variables are taken to be time-averaged quantities such that they can be more simply related to area.

First, we solve for Q using a simple relation for conservation of mass,

$$Q = PA \tag{A4}$$

where P is a spatially and temporally constant precipitation rate ($m \cdot yr^{-1}$) and A is upstream drainage area (m^2). This relation also assumes there is no effective subsurface water storage or input and no evapotranspiration.

Second, we use an empirical relation for hydraulic geometry,

$$W = k_w Q^b \tag{A5}$$

where $b \approx 0.5$. This equation has been found to be an appropriate relation for both alluvial and bedrock streams (Leopold and Maddock, 1953; Montgomery and Gran, 2001; Whipple, 2004).

Combining equations (A3), (A4), and (A5), fluvial erosion rate is recast as

$$E = KA^m S^n \tag{A6}$$

where $K = \frac{k_b P^{1/2}}{k_w}$, $m = 1/2$, and $n = 1$.

Hillslope erosion is simulated with an equation for linear diffusion in two horizontal dimensions (Culling, 1965):

$$E = -\kappa\left(\frac{\partial^2 h}{\partial x^2} + \frac{\partial^2 h}{\partial y^2}\right) \tag{A7}$$

where κ is a spatially constant diffusivity ($m^2 \cdot yr^{-1}$).

Combining equations (A6) and (A7) and a tectonic velocity field in a continuity equation for landscape evolution yields:

$$\frac{\partial h}{\partial t} = u + v\frac{\partial h}{\partial x} + \kappa\left(\frac{\partial^2 h}{\partial x^2} + \frac{\partial^2 h}{\partial y^2}\right) - KA^{1/2}S \tag{A8}$$

To further simplify analysis, we nondimensionalize equation (A8):

$$\frac{\partial h^*}{\partial t^*} = u^* + v^*\frac{\partial h^*}{\partial x^*} + \frac{\kappa}{TV}\left(\frac{\partial^2 h^*}{\partial x^{*2}} + \frac{\partial^2 h^*}{\partial y^{*2}}\right) - \frac{KT}{V}A^{*1/2}S \tag{A9}$$

which is further simplified as

$$\frac{\partial h^*}{\partial t^*} = \sin\alpha + \cos\alpha\frac{\partial h^*}{\partial x^*} + D\left(\frac{\partial^2 h^*}{\partial x^{*2}} + \frac{\partial^2 h^*}{\partial y^{*2}}\right) - N_e A^{*1/2}S \tag{A10}$$

Definitions of the nondimensional variables and parameters are given in Appendix DR3.

In our model, the average nondimensional horizontal node spacing is 0.5, simulation space is 8 units long in the y-direction and its width varies as a function of N_e and D. All four model boundaries are open, except in model 1f, in which case the lateral boundaries are reflected. In contrast to all of the other simulations, which use the landscape evolution model CHILD (Tucker et al., 2001), for model 1f we use the landscape evolution model GOLEM, which is based on a regular grid (Tucker and Slingerland, 1994).

APPENDIX DR3. Equations for nondimensional variables and parameters

Spatial variables: $x^* = \frac{x}{T}$, $y^* = \frac{y}{T}$, $h^* = \frac{h}{T}$, $A^* = \frac{A}{T^2}$

Velocity: $u^* = \frac{u}{V}$, $v^* = \frac{v}{V}$

Time: $t^* = \frac{tV}{T}$

Erosional parameters: $D = \frac{\kappa}{TV}$, $N_e = \frac{KT^{2m}}{V}$

Relief: $R_v^* = \frac{R_v}{R_v^0}$, $R_w^* = \frac{R_w}{R_w^0}$

Flux: $\phi^* = v^* \cdot R_w^* = \cos\alpha \cdot R_w^*$

APPENDIX DR4. Estimation of erosion number in Siwalik Hills

Fluvial erosion number, N_e, was estimated for the Siwalik Hills using available constraints on its component parameters and constants (K, T, V, and m). In the region of study in the Siwalik Hills, hanging wall velocity ranges from 4–21 mm/yr based on the records of deformed Holocene river terraces above the Main Frontal Thrust and Main Dun Thrust (Lavé and Avouac, 2000; Mugnier et al., 2004). Hanging-wall thickness ranges from ~4–6 km (Mugnier et al., 1999; Lavé and Avouac, 2000). In the eastern region, near the Bakeya and Bagmati Rivers, estimates of K fall in the range 1.47×10^{-4}–1.64×10^{-4} $m^{0.08}$/yr when $m = 0.46$ (Kirby and Whipple, 2001). Mean annual precipitation varies substantially across southern Nepal by a factor of ~4, indicating that the above value of K should also vary spatially, ignoring other factors such as lithology (Bookhagen et al., 2005). The eastern study area lies in a region of high precipitation rates relative to much of southern Nepal. Given that K scales with precipitation rate to a power of ~1/2 following the simplified formulation in Appendix DR2 (for a more complete derivation and formulation, see Whipple and Tucker, 1999), we might expect that K should vary due to precipitation by a factor of ~2. Bearing in mind that V and K are probably the least well-constrained parameters among our three sites, N_e likely falls between approximately 5 and 125.

APPENDIX DR5. Notation

x, y	horizontal dimensions, m
h	elevation of land surface, m
t	time, yr
v	horizontal component of bedrock velocity, m yr^{-1}
u	vertical component of bedrock velocity, m yr^{-1}
A	drainage area, m^2
Q	water discharge, m^3 yr^{-1}
W	stream width, m
S	stream channel gradient, unitless
m	area exponent in the stream-power erosion equation
T	thickness of hanging wall, m
V	bedrock velocity or slip rate above fault, m yr^{-1}
α	ramp dip, °
β	axial surface dip, °
κ	diffusivity, m^2 yr^{-1}
k_b	intrinsic bedrock incision coefficient, m^{-1}
k_w	channel width coefficient, $yr^{1/2}$ $m^{-1/2}$
b	channel width exponent, unitless
K	stream power coefficient, yr^{-1}
D	diffusion number, unitless
N_e	erosion number, unitless
r	Pearson product-moment correlation coefficient, unitless

R_w mean wind-gap relief, m

R_v mean cross-valley relief, m

R_w^0 mean wind-gap relief formed when ramp dip is 90°, m

R_v^0 mean cross-valley relief formed when ramp dip is 90°. m

R_w* nondimensional wind-gap relief, unitless

R_v* nondimensional cross-valley relief, unitless

ϕ* nondimensional lateral advection rate of relief across a ridge crest, unitless

TABLE DR1. CROSS-CORRELATION RESULTS FROM THE SIWALIK HILLS, NEPAL

Location	Coordinates		Convergence azimuth	α (°)[†]	*T* (km)[†]	*r*[§]	Length (km)	Maximum width	
	Lat. (°N)	Long. (°E)	(°)					South (km)	North (km)
Eastern									
A	27°15’	85°7’	~195	45	6	0.67	7.7	5	6
B	27°15’	85°12’	~195	40	5	0.89	5.0	3	5
C	27°12’	85°18’	~195	35	5	-0.02	4.7	4	5
D	27°11’	85°25’	~195	30	5	0.74	10.8	4	6
E	27°9’	85°35’	~195	30	5	0.26	13.0	4	5
Central									
F	27°50’	82°20’	~205	40	6	0.23	25.5	5	8
G	27°45’	82°45’	~205	40	5	0.13	22.5	7	4
Western									
H	28°45’	81°10’	~207	40	4	0.55	10.1	5	8
I	28°30’	81°35’	~207	35	4	-0.18	46.4	4	7
J	28°20’	81°35’	~207	30	4	0.30	33.6	4	4
Mean						0.36 ± 0.22[#]			

[†] Based on Lavé and Avouac (2000) and Mugnier et al. (1999).

[§] Pearson product-moment correlation coefficient (*r*) is calculated from paired vectors of mean elevations of opposing, whole ridge flanks.

[#] The distribution of *r* passes the Lilliefors goodness-of-fit test for a normal distribution (5% significance level). The reported confidence interval is 95%.

TABLE DR2. LIST OF MODEL PARAMETERS AND CROSS-CORRELATION RESULTS

Model code	N_e	D	α (°)	T (km)	$r^{\dagger}$ mean	$r^{\dagger}$ 95% confidence interval	n
Vertical uplift simulations							
1a (*null hypothesis*)	10	0	90	10.0	0.118	0.027	200
1b	10	0	90	15.0	0.149	0.031	200
1c	10	0	90	20.0	0.090[§]	0.033	200
1d	100	0	90	10.0	0.148	0.027	200
1e	10	10^{-1}	90	10.0	0.121	0.031	200
1f[#]	10	0	90	10.0	0.118	0.041	100
Fault-bend fold simulations							
2a	2	0	30	5.0	0.547	0.073	10
2b	3	0	30	5.0	0.509	0.073	10
2c	5	0	30	5.0	0.338	0.070	10
2d	10	0	30	5.0	0.229	0.126	10
2e	15	0	30	5.0	0.134	0.111	10
2f	50	0	30	5.0	0.192	0.105	10
2g	100	0	30	5.0	0.117	0.105	10
3a	10	10^{-5}	30	5.0	0.230	0.121	10
3b	10	10^{-4}	30	5.0	0.224	0.127	10
3c	10	10^{-3}	30	5.0	0.207	0.107	10
3d	10	10^{-2}	30	5.0	0.262	0.135	10
3e	10	10^{-1}	30	5.0	0.280	0.108	10
3f	10	10^{0}	30	5.0	0.324	0.108	10
3g	10	10^{1}	30	5.0	0.524	0.046	10
4a	10	0	10	1.7	0.042	0.102	10
4b	10	0	20	3.4	0.150	0.068	10
4c	10	0	30	5.0	0.195	0.077	10
4d	10	0	40	6.4	0.182	0.087	10
4e	10	0	50	7.7	0.193	0.105	10
4f	10	0	60	8.7	0.122	0.100	10
4g	10	0	70	9.4	0.089	0.103	10
4h	10	0	80	9.9	0.020	0.109	10
5a	5	0	10	1.7	0.191	0.141	10
5b	5	0	20	3.4	0.267	0.057	10
5c	5	0	30	5.0	0.299	0.104	10
5d	5	0	40	6.4	0.360	0.120	10
5e	5	0	50	7.7	0.294	0.099	10
5f	5	0	60	8.7	0.252	0.124	10
5g	5	0	70	9.4	0.258	0.114	10
5h	5	0	80	9.9	0.099	0.086	10

[†] Correlation coefficient is calculated for mean elevations of entire ridge flanks.

[§] The distribution is not normal as determined by the Lilliefors test at the 5% significance level. The p-value of this individual test is 0.035.

[#] Model 1f differs from 1a in that 1a has lateral boundaries at fixed elevations and model 1f has reflected boundaries, which wrap around and are continuous with the opposite edge. In contrast to all other model runs, this was conducted using the landscape evolution model GOLEM, which is based on a regular grid (Tucker and Slingerland, 1994).

REFERENCES CITED

Bookhagen, B., Thiede, R.C., and Strecker, M.R., 2005, Abnormal monsoon years and their control on erosion and sediment flux in the high, arid Northwest Himalaya: Earth and Planetary Science Letters, v. 231, p. 131-146.

Borradaile, G., 2003, Statistics of Earth Science Data: Berlin, Springer-Verlag, 351 p.

Culling, W.E.H., 1965, Theory of erosion on soil-covered slopes: Journal of Geology, v. 73, p. 230-254.

Davis, J.C., 1973, Statistics and Data Analysis in Geology: New York, John Wiley and Sons, 550 p.

Howard, A.D., Dietrich, W.E., and Seidl, M.A., 1994, Modeling fluvial erosion on regional to continental scales: Journal of Geophysical Research, v. 99, p. 13,971-13,986.

Kirby, E., and Whipple, K., 2001, Quantifying differential rock-uplift rates via stream profile analysis: Geology, v. 29, p. 415-418.

Lavé, J., and Avouac, J.P., 2000, Active folding of fluvial terraces across the Siwaliks Hills, Himalayas of central Nepal: Journal of Geophysical Research, v. 105, p. 5735-5770.

Leopold, L.B., and Maddock, T., Jr., 1953, The hydraulic geometry of stream channels and physiographic implications: U. S. Geological Survey Professional Paper 252, p. 57.

Montgomery, D.R., and Gran, K.B., 2001, Downstream variations in the width of bedrock channels: Water Resources Research, v. 37, p. 1841-1846.

Mugnier, J.-L., Huyghe, P., Leturmy, P., and Jouanne, F., 2004, Episodicity and rates of thrust-sheet motion in the Himalayas (western Nepal), *in* McClay, K.R., ed., AAPG Memoir, v. 82, p. 91-114.

Mugnier, J.L., Leturmy, P., Mascle, G., Huyghe, P., Husson, L., Chalaron, E., Vidal, G., and Delcaillau, B., 1999, The Siwaliks of western Nepal; I, Geometry and kinematics: Journal of Asian Earth Sciences, v. 17, p. 629-642.

Suppe, J., 1983, Geometry and kinematics of fault-bend folding: American Journal of Science, v. 283, p. 684-721.

Tucker, G.E., Lancaster, S.T., Gasparini, N.M., Bras, R.L., and Rybarczyk, S.M., 2001, An object-oriented framework for distributed hydrologic and geomorphic modeling using triangulated irregular networks: Computers & Geosciences, v. 27, p. 959-973.

Tucker, G.E., and Slingerland, R.L., 1994, Erosional dynamics, flexural isostasy, and long-lived escarpments; a numerical modeling study: Journal of Geophysical Research, v. 99, p. 12,229-12,243.

Whipple, K.X., 2004, Bedrock rivers and the geomorphology of active orogens: Annual Review of Earth and Planetary Sciences, v. 32, p. 151-185.

Whipple, K.X., and Tucker, G.E., 1999, Dynamics of the stream-power river incision model; implications for height limits of mountain ranges, landscape response timescales, and research needs: Journal of Geophysical Research, v. 104, p. 17,661-17,674.

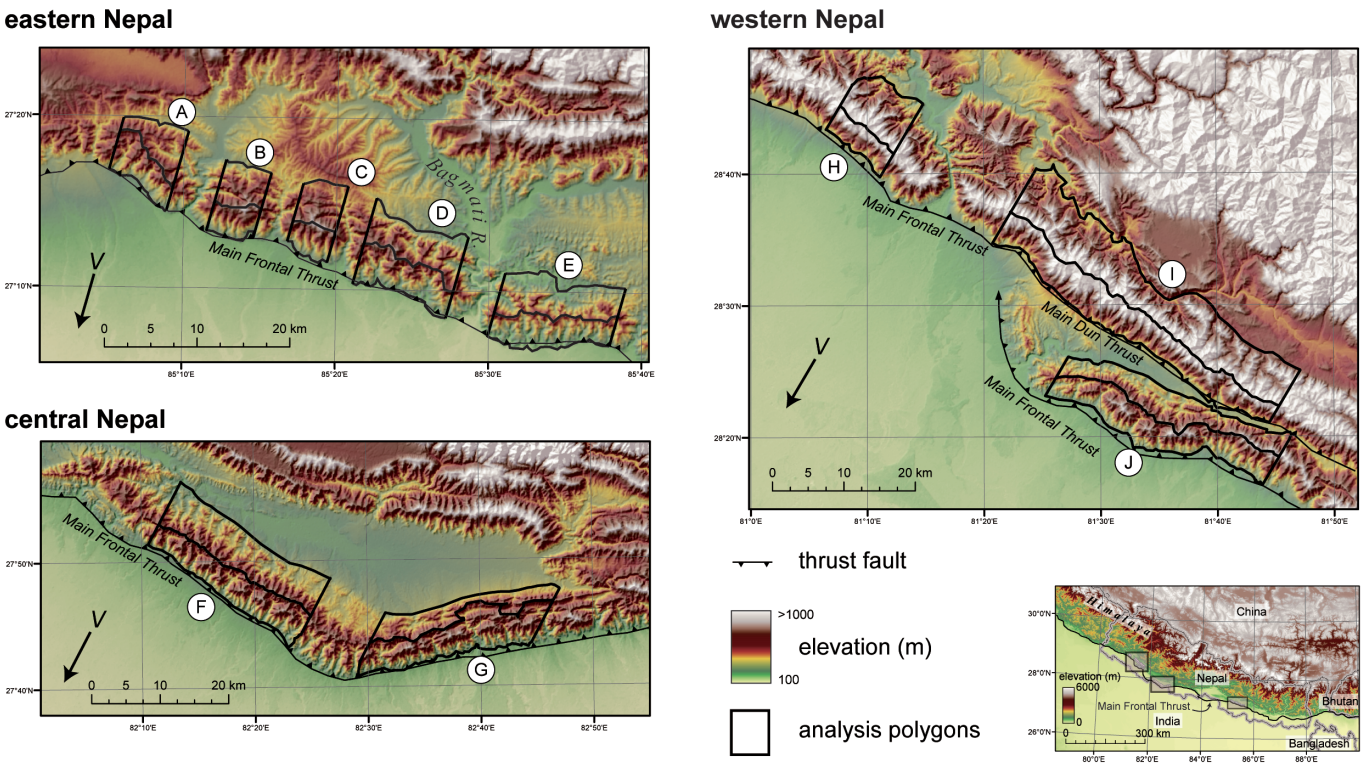

Figure DR1. Shaded relief maps from eastern, central, and western Nepal showing locations along the Siwalik Hills that were used in topographic cross-correlations, marked with black polygons. Location map is at bottom right with black boxes representing the three regions. Direction of hanging wall transport (or convergence) is shown with an arrow labeled *V*.

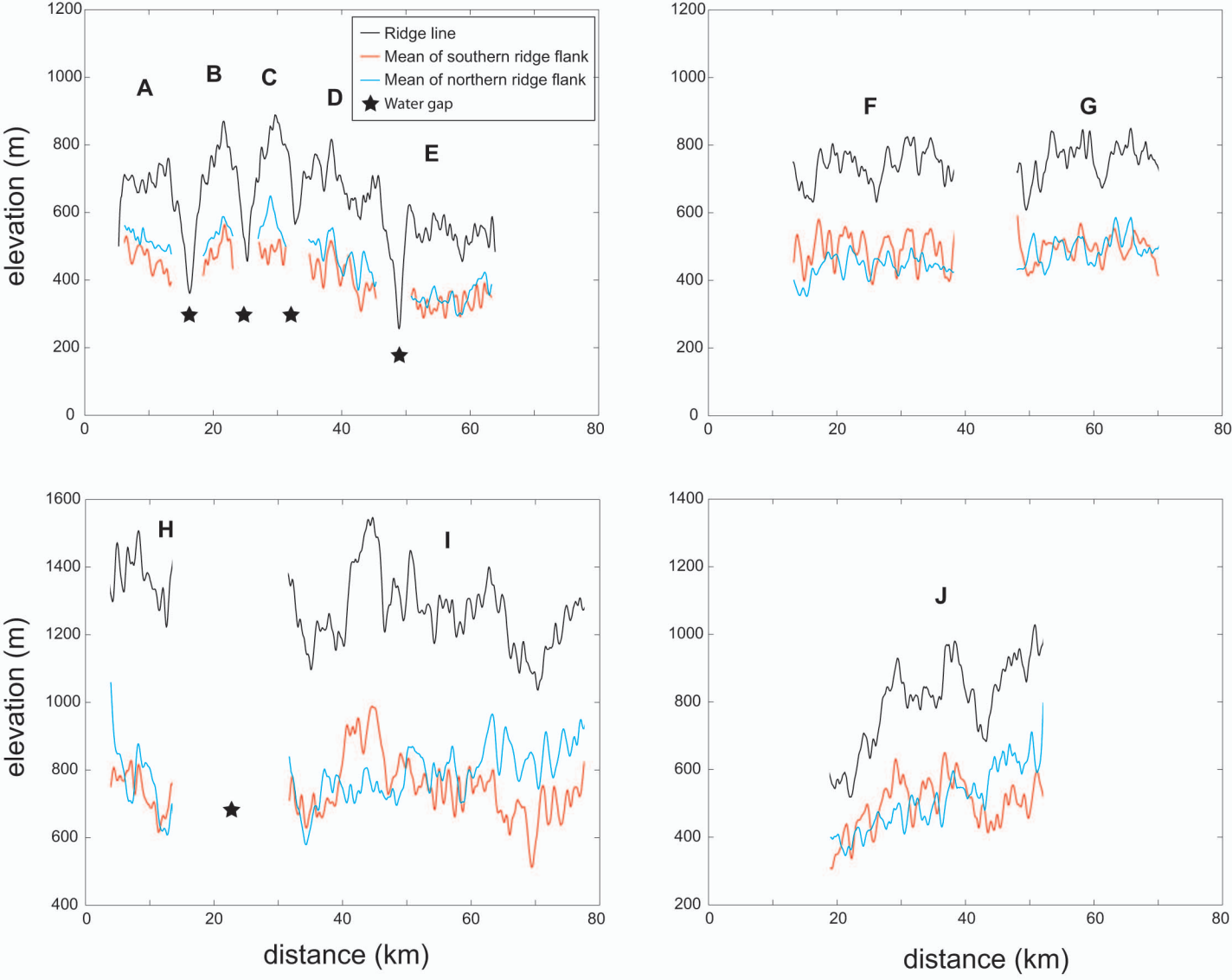

Figure DR2. Elevation profiles measured perpendicular to the convergence direction of the hanging wall. Ridge profiles are shown in black. Profiles in red and blue represent the mean elevations of the southern (red) and northern (blue) flanks of the ridge. Breaks in profiles are located at water gaps and bends in the ridge. Profiles have been smoothed with a 500-m wide moving window to reduce local topographic noise (produces topographic roughness comparable to the model with a 500 m node spacing). Locations of these profiles are shown in Figure DR1.

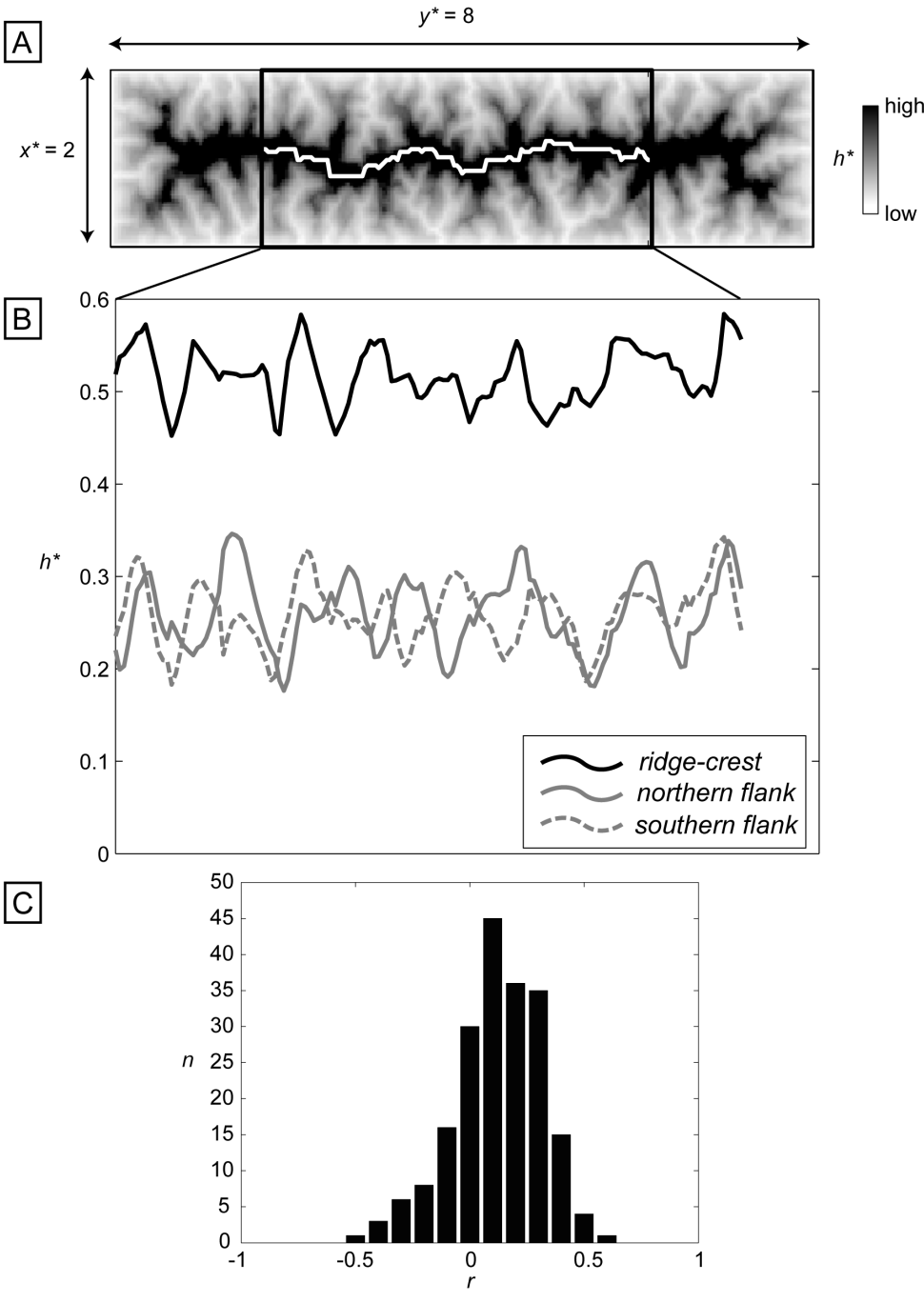

Figure DR3. Results of the vertical rock uplift model (model 1a). (A) Elevation map, in which darker shades indicate higher elevations. Ridge line is marked in white. (B) Topographic profiles of the ridge line and mean elevations from the "southern" and "northern" flanks of the ridge, in which elevations are averaged along columns. (C) Histogram of *r* from 200 realizations of model 1a.